Reassessment of the Dynamic Thermomechanical Conversion in Metals

J. C. Nieto-Fuentes,[1,*] S. Osovski,[1] A. Venkert,[2] and D. Rittel[1]
[1]Faculty of Mechanical Engineering, Technion, 320000 Haifa, Israel
[2]Chemistry Department, NRCN, 84190 Beer Sheva, Israel

(Received 17 July 2019; published 20 December 2019)

Heat dissipation still remains an unsolved problem in dynamic plasticity, where nearly adiabatic conditions prevail during high-rate loading scenarios. It is well known that the mechanical energy that is not dissipated as heat during material straining remains stored in the lattice as microstructural defects, and thus, a one-to-one relationship can be expected between the stored energy, the materials microstructure, and its mechanical characteristics. This work demonstrates that this is not so straightforward. High-rate experiments on a Kolsky bar, combined with *in situ* thermal measurements, were performed on two well-studied materials: pure nickel and aluminum. A dislocation-based constitutive model was used to estimate the mechanical and thermomechanical material behavior. For both materials, the thermal response was observed to be strongly strain rate sensitive, while the mechanical flow, and microstructural characteristics (as characterized by transmission electron microscopy at similar strains), were not. This apparent discrepancy between mechanical and microstructural vs thermal results is discussed, and the concept of thermomechanical conversion is reassessed.

DOI: 10.1103/PhysRevLett.123.255502

Dynamic (impact) failure of metallic solids may result in many, often unexpected accidental situations. Under such circumstances, one can observe specific dynamic deformation mechanisms. The short time scale of the dynamic loading is responsible for a temperature rise of the material due to the (near) adiabaticity of the problem [1]. One direct consequence of this phenomenon may be the potential thermal softening of the material and subsequent localization of the deformation, into the so-called adiabatic shear bands [2]. Despite this, not all of the mechanical energy spent into inelastic straining is converted into heat, and a further fraction—commonly known as the stored energy of cold work (SECW) [3]—remains stored in the material, particularly in the form of microstructural defects and arrangement thereof. Thus, one can calculate the fraction of inelastic work dissipated as heat—generally called the Taylor-Quinney factor [4,5] (TQF or β_{int})—just by solving the heat conduction equation, which after neglecting thermoelastic heating and assuming adiabatic conditions, reads [5]

$$\beta_{\text{int}} = \frac{\rho C \Delta T}{\int \sigma_{ij} d\varepsilon_{ij}^{P}} = \frac{Q}{W_p}, \tag{1}$$

where ρ is the material density, C is the heat capacity, ΔT is the temperature rise, σ_{ij} and ε_{ij}^{P} are the components of the stress and plastic strain tensors, respectively; Q is the energy dissipated as heat, and W_p is the plastic or mechanical work.

Several earlier works [6–12] have identified the SECW—which can be calculated as the "1-β_{int}" fraction of the mechanical work—as a potential triggering mechanism for microstructural softening under dynamic conditions, which inevitably precedes material failure by shear localization. Less was reported in the literature about the rate sensitivity of the energy storage (or the heat dissipation), although a few works have partly addressed this issue [13–16]. Considering the significance of the thermomechanical coupling in dynamic material failure, one may wonder about the extent to which the stored energy of cold work can be uniquely predicted from a microstructural point of view.

It is well known that the amount of energy stored in a plastically deformed material is directly proportional to the evolving density of dislocations, inasmuch as these are the main contribution to the former [17]. The expression for estimating the volumetric stored energy in the material, where only short-range dislocation-dislocation interactions are considered, can be expressed as [18]

$$E_{\text{stored}} = \frac{1}{4\pi k} \ln\left(\frac{1}{2b\sqrt{\rho_{\text{tot}}}}\right) G b^2 \rho_{\text{tot}}, \tag{2}$$

where k is 1 or $(1-\nu)$, depending on the type of the dislocation (ν being the Poissons ratio); b is the Burgers vector, G is the shear modulus, and ρ_{tot} is the total line dislocation density. Assuming a realistic value for the Burgers vector (2.5 Å), setting $k = 1$, and varying the dislocation density between 10^{10} and 10^{15} m^{-2} (which may be characteristic of several processes of plastic

deformation), the term "$1/(4\pi k)\ln[1/(2b\sqrt{\rho_{\mathrm{tot}}})]$" is shown to vary from 0.8 to 0.3. Consequently, Eq. (2) becomes [19]

$$E_{\mathrm{stored}} = \alpha G b^2 \rho_{\mathrm{tot}}, \tag{3}$$

where α is a constant of the order of 0.5, adjusted depending on the material. An estimation of the energy stored in a statically deformed metal, using two different dislocation-based hardening models, was done in [20], where a variant of Eq. (2) was used to compare the obtained analytical values with the measured ones from differential scanning calorimetry (DSC). Though slightly underestimated, the predicted stored energy values were in good agreement with those measured by DSC. As to its dynamic counterpart, the stored energy of a dynamically deformed material was calculated by other authors through the measured increase of temperature during high speed deformation [21,22]. There, the analytical estimation based on dislocation mechanics completely disagreed with the measured values of the energy storage. Specifically, in [22], the suitability of using Eq. (3) [or either Eq. (2)] to calculate the SECW (and, by consequence, the TQF) under dynamic conditions was called into question. A different approach, based on the nonequilibrium thermodynamic theory of dislocation plasticity of Langer *et al.* [23–25], was applied in [26] on a finite element framework to locally compute the TQF for an adiabatic shear banding problem.

In this Letter, we show, by means of a counter-example, that there is no unique and unequivocal relationship between the stress-strain characteristics and, hence, the final microstructure of a dynamically deformed material and its energy storing (thus, dissipation) capacity. A dislocation-based constitutive model is used to estimate the thermomechanical response of two well-studied metallic materials (nickel and aluminum), which were further tested in an extensive experimental campaign under high-rate deformation. The studied high-purity nickel alloy is totally characterized, while pure aluminum is only shown to demonstrate that the observation is not restricted to the former.

A brief discussion about the mechanical model is presented here, with details provided in [22]. The material model itself considers dislocation cell structures and their evolution, in a two-phase approach: cell walls and cell interiors [27–30]. The former constitutes the hard phase, where dislocations are trapped, and therefore, their density is higher; the latter, in comparison with the cell walls, are nearly dislocation free. To accommodate gradients of plastic strain (lattice curvature) during deformation, the presence of geometrically necessary dislocations (GNDs) in the walls is considered too. Each population of dislocations has its own evolution expression, which, combined by a rule of mixtures, allows us to calculate the total dislocation density

$$\rho_{\mathrm{tot}} = f(\rho_w + \rho_{\mathrm{GND}}) + (1-f)\rho_c, \tag{4}$$

where ρ_w is the line dislocation density of the cell walls, ρ_c its counterpart of the cell interiors, ρ_{GND} is the line dislocation density of GNDs, while f is the volume fraction of the cell walls. A certain density of line defects in the microstructure will turn into a flow resistance at the macroscopic level, which, under uniaxial loading and adopting the Taylor averaging model [31], reads

$$\sigma = M(\tau_0 + \tau), \tag{5}$$

where M is the Taylor factor (equal to 3.06 for most fcc materials), τ_0 is a constant threshold lattice resistance ($\tau_0 = \sigma_0/M$), and τ is the shear strength of the cell, which can be determined as

$$\tau = \alpha G b[f\sqrt{\rho_w} + (1-f)\sqrt{\rho_c}]. \tag{6}$$

Additional terms, such as temperature or strain rate sensitivity effects, may be included in Eq. (6) [22].

Therefore, the denominator of the TQF [Eq. (1)] can be defined utilizing Eq. (5). To complete the expression analytically, and since no information about the temperature increment is provided, a thermodynamically consistent heat generation is needed. In this work, we have used the formulation provided by Hakansson *et al.* [32], which is based on a crystal plasticity framework and was derived considering the latent hardening into the free energy function. Using Taylor homogenization, i.e., considering all slip systems as equally active during deformation, and dividing the slip resistance into lattice friction (τ_0) and hardening [Eq. (6)], the evolution of the heat dissipation with the microscopic strain can be computed as

$$\frac{dQ}{d\gamma} = |\tau_0 + \tau - \tau_b|\left(1 - \frac{\tau}{\tau_0+\tau} + B\frac{\tau}{\tau_0+\tau}g\right) + \chi\tau_b^2, \tag{7}$$

where τ_b is the back stress, χ, here, is a factor controlling the amount of dissipated energy related to the back stress; B is a material parameter connected with the saturation of the slip resistance, g, the strain evolution of which follows:

$$\frac{dg}{d\gamma} = (1 - Bg)\frac{|\tau_0 + \tau - \tau_b|}{\tau_0 + \tau}. \tag{8}$$

The evolution of the back stress, resulting from incompatibility in plastic deformation, i.e., internal stresses produced by the difference in the dislocation densities between the cell walls and the cell interiors, can be calculated as [33]

$$\frac{d\tau_b}{d\gamma} = k_r \frac{f}{1-f}\alpha G b(\sqrt{\rho_w + \rho_{\mathrm{GND}}} - \sqrt{\rho_c}) - k_r\tau_b, \tag{9}$$

where k_r is a constant controlling the back-stress recovery. Introducing the effect of internal stresses in the formulation provides information about the distribution of dislocations

TABLE I. Summary of the parameters used in the calculation of the heat dissipation [Eq. (7)].

	B	g_{initial}	$\chi(\text{Pa}^{-1})$	k_r
Ni200	0.3	0.007	5e-10	40
Al99.99%	0.7	0.007	1e-9	40

in the material, an approach that was already shown to give reasonable results on the prediction of the heat dissipation in dislocation dynamics calculations [34]. A summary of the parameters used to calculate Eq. (7), selected in accordance to experimental observations, can be found in Table I.

Concerning the experimental procedure, thermomechanical compression testing under high rate deformation was conducted on a split Hopkinson pressure bar (SHPB), made of ϕ19.4 mm C300 hardened maraging steel bars, combined with *in situ* thermal measurements by infrared (IR) detection. A 2-photoconductor high-speed IR detector (HgCdTe and InSb), along with a 1:1 magnification optical system, was located facing the specimen. The data acquisition frequency of 2 MHz was fast enough to capture the transient events under SHPB testing. Radiation emitted from the specimen was collected by the IR detector, giving rise to a voltage signal, further reduced into the specimen's surface temperature—see also [22]. Analogous configurations for high-speed thermal measurements were reported to succeed in previous works of these and other authors, e.g., [14,16,22,35–41].

Cylinders for uniaxial SHPB compression loading were carefully machined from a ϕ12 mm Ni200 bar, in the as-received condition, and from an ingot of as-cast pure aluminum (Al 99.99%). Electron backscatter diffraction (EBSD) analyses were performed on the original materials following standard polishing procedures, with an Oxford NordlysNano detector in a Tescan MIRA-3 FEG scanning electron microscope. A proper selection of the EBSD step size during the scan was chosen to be at least 1/10 of the average grain size, leading to values of 0.7 μm for nickel and 20 μm for aluminum. After postprocessing EBSD data with MTEX software [42], the grain distribution map and pole figures were extracted—see Figs. 1(a) and 1(d). The average grain size was determined as 7.9 μm for Ni200 and 1.6 mm for pure aluminum. Ni200 samples for EBSD analysis were extracted from planes both parallel and perpendicular to the bar axis and no difference between them was found.

Ni200 specimens were machined in two different sets of lengths and diameters: $L5\phi5$ mm and $L6\phi6$ mm, while

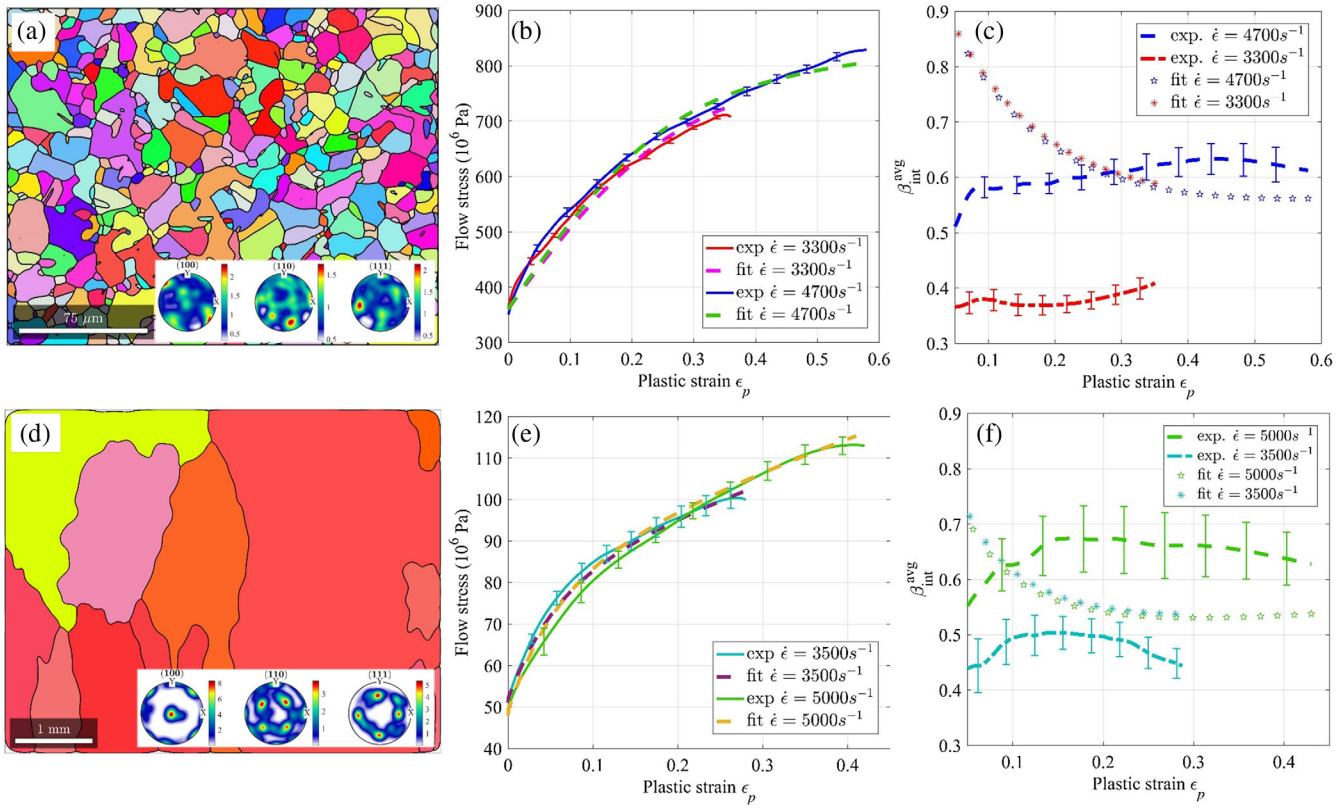

FIG. 1. Grain orientation maps, averaged stress vs plastic strain [both experimental and predicted by Eq. (5)], and averaged Taylor-Quinney factors (β_{int}) vs plastic strain [both experimental and predicted by Eqs. (1) and (7)], for (a)–(c) Ni200 and (d)–(f) Al99.99%. Experimental curves contain standard error bars.

aluminum specimens were manufactured in a $L8\phi8$ mm configuration. The 31 most representative samples (showing an accurate time synchronization [43] in the SHPB and IR recorded signals) of the experimental campaign were chosen for this study, and can be classified into independent groups of strain rates (see Table II): 3300 s^{-1} (numbers 1 to 10) and 4700 s^{-1} (numbers 11 to 18) for Ni200, and 3500 s^{-1} (numbers 19 to 25) and 5000 s^{-1} (numbers 26 to 31) for pure aluminum. In addition, two Ni200 samples for transmission electron microscopy (TEM) were deformed in interrupted tests up to a strain of 0.2—see the bright field TEM images in Figs. 2(a) and 2(c). Thin foils were extracted from planes perpendicular to the bar (specimen) axis.

Figure 1(b) shows the averaged mechanical response of Ni200 for the two strain rates under study. Though quite scarce in literature, comparable experimental results for analogous high-purity nickel can be found [44,45]. A very similar work hardening behavior for both deformation velocities (strain rates) is evident here, indicating an apparent lack of strain rate sensitivity of the material in the high-rate regime, noting that strain rate effects in nickel may be more apparent when the initial grain size is scaled down to the nanocrystalline level [45,46]. A comparable trend in terms of strain-rate sensitivity was observed for pure aluminum—see Fig. 1(e), akin to the experimental results of other authors [40,47]. Here, we remark that the final microstructures of Ni200 (at a strain of 0.2) for both strain rates were similar, showing equiaxed dislocation cell structures with tangled boundaries, as known to form in deformed nickel [48]. No signs of recrystallization or other energy-consuming phenomenon were observed, as shown in Figs. 2(a) and 2(c). The dislocation density was estimated from EBSD analysis [49] in the deformed specimens showing that, for both strain rates, the overall distribution is absolutely comparable [see Figs. 2(b) and 2(d)]—thus, supporting both the TEM results and the analytical modeling. Specifically, the final average dislocation density for Ni200 samples deformed at a strain of 0.2 was determined to be $(3.46 \pm 2.32) \times 10^{14}$ m^{-2} at 3300 s^{-1}, and $(3.51 \pm 2.41) \times 10^{14}$ m^{-2} at 4700 s^{-1}. Following the similarities in the statistical characteristics of the dislocation density distributions, we further examined the distribution function by calculating their distance from each other utilizing Bhattacharyyas distance [50].

TABLE II. Summary of the specimens' dimensions and experimental strain rates for Ni200 (N prefix) and pure aluminum (A prefix).

No.	Spec.	L-ϕ(mm)	$\dot{\epsilon}(s^{-1})$
1	N20	4.97–5.01	3260
2	N22	4.97–5.00	3370
3	N24	5.06–4.97	3240
4	N25	5.00–5.00	3260
5	N67	5.98–5.97	3330
6	N77	4.94–5.01	3320
7	N78	4.95–5.01	3230
8	N81	4.90–5.02	3300
9	N83	5.00–5.00	3290
10	N85	4.96–5.00	3270
11	N28	5.00–5.00	4690
12	N29	5.00–5.00	4730
13	N30	5.05–5.02	4700
14	N32	5.06–5.00	4690
15	N33	5.02–5.00	4770
16	N34	5.03–5.00	4600
17	N39	4.93–5.00	4750
18	N42	4.87–4.97	4790
19	A32	8.01–8.00	3560
20	A36	8.04–8.00	3360
21	A37	8.01–7.98	3550
22	A40	8.02–8.00	3550
23	A41	8.01–8.04	3380
24	A42	8.00–7.98	3500
25	A43	7.98–7.98	3650
26	A53	7.92–8.00	5060
27	A55	8.04–7.96	4920
28	A56	7.84–7.98	4900
29	A58	8.04–8.07	4870
30	A59	8.00–8.00	5240
31	A60	8.04–7.98	5280

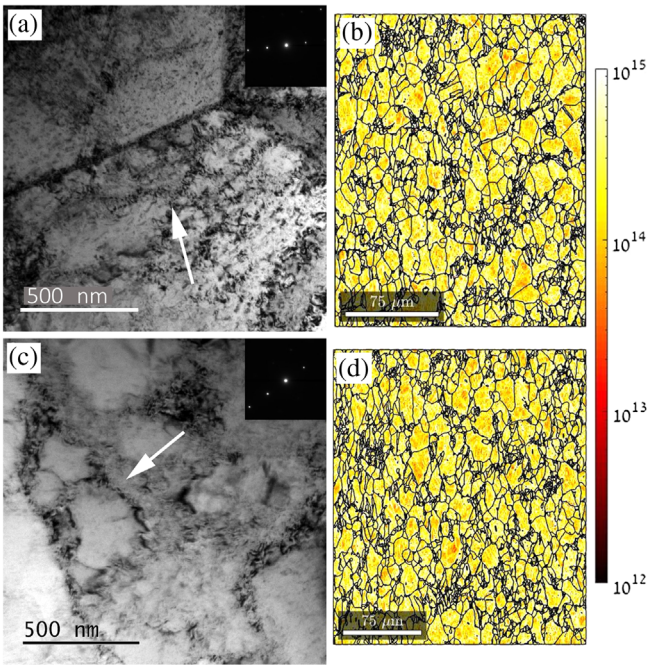

FIG. 2. Bright field TEM images showing the microstructure of Ni200 after 20% plastic deformation at: (a) strain rate 3300 s^{-1} and (c) strain rate 4700 s^{-1} (tangled dislocation boundaries are indicated by arrows, and the corresponding diffraction patterns are embedded in the figure). Dislocation density estimation (scale in m^{-2}) via EBSD analysis at: (b) strain rate 3300 s^{-1} and (d) strain rate 4700 s^{-1}.

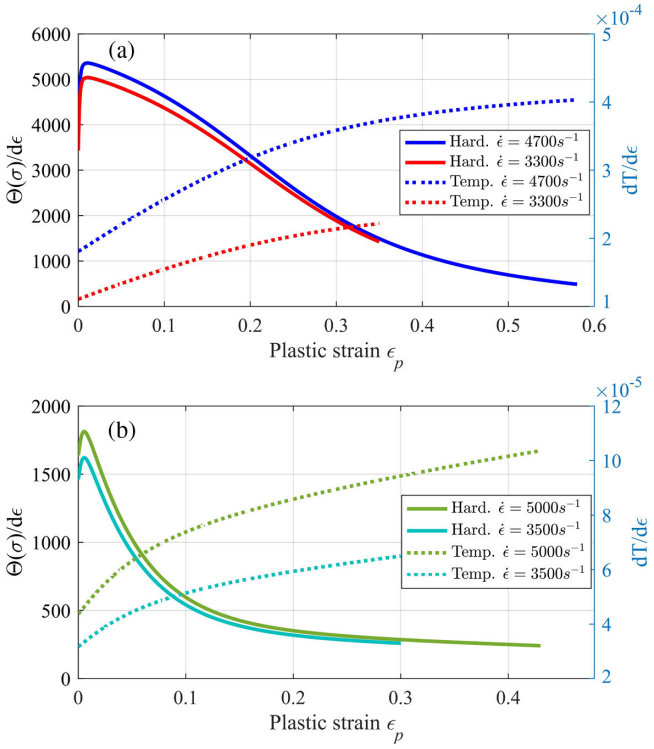

FIG. 3. Incremental hardening and temperature rise vs plastic strain, for (a) Ni200 and (b) Al99.99%.

The latter was estimated as 8×10^{-3}, indicating that the two are practically identical irrespective of the strain rate, thus, leading to the conclusion that the levels of stored energy are identical as well.

Figures 1(c) and 1(f) show the evolution of the inelastic heat fraction (β_{int}) during deformation. In this aspect, Ni200 and pure aluminum exhibit a definite thermomechanical sensitivity to the applied strain rate, in the sense that the amount of dissipated heat varies notably, e.g., for nickel, between 35% and 40% for the 3300 s^{-1} case, and between 55% and 65% when the material is deformed at 4700 s^{-1}. Similar trends were obtained for aluminum. It can be noted that the thermal strain rate sensitivity is absolutely not captured by the dislocation-based model, whereas the mechanical response is properly estimated—see Figs. 1(b) and 1(e).

These results lead to the following question: on what physical grounds can a material that exhibits comparable dynamic mechanical properties irrespective of the strain rate and the microstructure be creating such a contrasting amount of thermal power (heat rate) in each situation?

Other authors have reported, without further emphasis, a similar anomaly [15] where the dynamic thermomechanical response of an aluminum alloy was compared for several but close values of strain rate. The considerable thermal sensitivity presented there (TQFs varying between 0.4 and 0.95) is oppositely accompanied by milder changes in the mechanical flow characteristics; on the other hand, no microstructural data were collected there; thus, a direct comparison with the work presented here is precluded. In the cases studied in this Letter, the rates of hardening for the two different strain rates in both materials were almost equal, respectively, as shown in Fig. 3. Yet, from the temperature rise per strain increment (in the same figure), one clearly sees that the heat generation rate surpasses the energy storing rate capacity of the material as the strain rate increases. Since no evident distinction between the final microstructure at the two strain rates was found (see Fig. 2), these observations can be understood as a counterexample of β_{int} being solely a result of the final microstructure without accounting for its evolutions. Note, here, the claim made by Taylor and Quinney in 1934 [4], suggesting the influence of microstructural aspects on the material energy storage behavior prior to failure, a fact that has been lightly touched upon in literature since then.

While it would be highly desirable to monitor microstructural evolutions in real time at the dislocation scale, this eventuality is not achievable by current experimental means. Yet, some conclusions can be drawn from the present observations, namely: (a) the dislocation model adequately describes the mechanical behavior of the two metals in question at both strain rates, while the thermal response—especially concerning the strain rate sensitivity—is not properly captured; (b) for the pure fcc metals studied here, there is no definite or unique relationship between the mechanical response (thus, the final microstructure) and the stored energy of a dynamically deformed material; (c) the TQF is suggested to be rather influenced by the evolution of the microstructure and not by a final state of equilibrium, as commonly assumed, suggesting that dislocation kinetics and the dislocation structures' evolution are of prime importance for understanding nonequilibrium deformation states and thermal dissipation, as suggested by Langer *et al.* [23].

The research leading to these results has received funding from the European Union Horizon 2020 Program (Excellent Science, Marie-Sklodowska-Curie Actions) under REA Grant Agreement No. 675602 (Project OUTCOME).

*Corresponding author.
juan-carlos@campus.technion.ac.il

[1] B. A. Boley and J. H. Weiner, *Theory of Thermal Stresses* (John Wiley & Sons, New York, 1960), p. 586.
[2] C. Zener and J. H. Hollomon, J. Appl. Phys. **15**, 22 (1944).
[3] M. B. Bever, D. L. Holt, and A. L. Titchener, Prog. Mater. Sci. **17**, 5 (1973).
[4] G. I. Taylor and H. Quinney, Proc. R. Soc. A **143**, 307 (1934).
[5] D. Rittel, Mech. Mater. **31**, 131 (1999).
[6] H. A. Padilla, C. D. Smith, J. Lambros, A. J. Beaudoin, and I. M. Robertson, Metall. Mater. Trans. A **38**, 2916 (2007).
[7] S. Osovski, D. Rittel, P. Landau, and A. Venkert, Scr. Mater. **66**, 9 (2012).

[8] S. Osovski, D. Rittel, and A. Venkert, Mech. Mater. **56**, 11 (2013).
[9] D. Rittel, P. Landau, and A. Venkert, Phys. Rev. Lett. **101**, 165501 (2008).
[10] X. Liu, Y. Zhou, X. Zhu, D. Wang, and Q. Fan, Mater. Sci. Eng. A **746**, 322 (2019).
[11] D. Rittel, Z. G. Wang, and M. Merzer, Phys. Rev. Lett. **96**, 075502 (2006).
[12] Y. Guo, Q. Ruan, S. Zhu, Q. Wei, H. Chen, J. Lu, B. Hu, X. Wu, Y. Li, and D. Fang, Phys. Rev. Lett. **122**, 015503 (2019).
[13] D. A. S. Macdougall, Exp. Mech. **40**, 298 (2000).
[14] J. J. Mason, A. J. Rosakis, and G. Ravichandran, Mech. Mater. **17**, 135 (1994).
[15] T. Zhang, Z. R. Guo, F. P. Yuan, and H. S. Zhang, Acta Mech. Sin. **34**, 327 (2017).
[16] D. Ghosh, O. T. Kingstedt, and G. Ravichandran, Metall. Mater. Trans. A **48**, 14 (2017).
[17] A. L. Titchener and M. B. Bever, Acta Metall. **8**, 338 (1960).
[18] J. P. Hirth and J. Lothe, *Theory of Dislocations*, 2nd ed. (Wiley-Interscience, New York, 1982).
[19] D. Hull and D. J. Bacon *Introduction to Dislocations*, 5th ed. (Butterworth-Heinemann, Amsterdam, 2011), p. 272.
[20] M. Čebron and F. Kosel, J. Mech. Eng. **60**, 462 (2014).
[21] R. Kapoor and S. Nemat-Nasser, Mech. Mater. **27**, 1 (1998).
[22] J. C. Nieto-Fuentes, D. Rittel, and S. Osovski, Int. J. Plast. **108**, 55 (2018).
[23] J. S. Langer, E. Bouchbinder, and T. Lookman, Acta Mater. **58**, 3718 (2010).
[24] J. S. Langer, Phys. Rev. E **94**, 063004 (2016).
[25] J. S. Langer, Phys. Rev. E **95**, 013004 (2017).
[26] C. K. C. Lieou, H. M. Mourad, and C. A. Bronkhorst, Int. J. Plast. **119**, 171 (2019).
[27] Y. Estrin, L. S. Toth, A. Molinari, and Y. Bréchet, Acta Mater. **46**, 5509 (1998).
[28] Y. Estrin, L. S. Toth, Y. Bréchet, and H. S. Kim, Mater. Sci. Forum **503–504**, 675 (2006).
[29] H. Parvin and M. Kazeminezhad, Comput. Mater. Sci. **95**, 250 (2014).
[30] F. Liu, H. Yuan, J. Yin, and J. T. Wang, Mater. Sci. Eng. A **662**, 578 (2016).
[31] U. F. Kocks and H. Mecking, Prog. Mater. Sci. **48**, 171 (2003).
[32] P. Håkansson, M. Wallin, and M. Ristinmaa, Int. J. Solids Struct. **45**, 1570 (2008).
[33] E. Chen, L. Duchêne, A. M. Habraken, and B. Verlinden, J. Mater. Sci. **45**, 4696 (2010).
[34] A. A. Benzerga, Y. Bréchet, A. Needleman, and E. Van der Giessen, Acta Mater. **53**, 4765 (2005).
[35] D. Rittel, A. A. Kidane, M. Alkhader, A. Venkert, P. Landau, and G. Ravichandran, Acta Mater. **60**, 3719 (2012).
[36] D. Rittel and Z. G. Wang, Mech. Mater. **40**, 629 (2008).
[37] L. H. Zhang, D. Rittel, and S. Osovski, Mater. Sci. Eng. A **729**, 94 (2018).
[38] D. Rittel, L. H. Zhang, and S. Osovski, J. Mech. Phys. Solids **107**, 96 (2017).
[39] G. Ravichandran, A. J. Rosakis, J. Hodowany, and P. Rosakis, in AIP Conf. Proc. **620**, 557 (2002).
[40] J. Hodowany, G. Ravichandran, A. J. Rosakis, and P. Rosakis, Exp. Mech. **40**, 113 (2000).
[41] D. Rittel, G. Ravichandran, and A. Venkert, Mater. Sci. Eng. A **432**, 191 (2006).
[42] F. Bachmann, R. Hielscher, and H. Schaeben, Solid State Phenom. **160**, 63 (2010).
[43] The strain gages and the IR signals are recorded at different locations, and need to be carefully synchronized using the sound wave velocity in the bars [see Fig. 6(a) and explanations in Ref. [22]].
[44] P. S. Follansbee, J. C. Huang, and G. T. Gray, Acta Metall. Mater. **38**, 1241 (1990).
[45] S. Rajaraman, K. N. Jonnalagadda, and P. Ghosh, in Dynamic Behavior of Materials (2013), Vol. **1**, pp. 157–163.
[46] F. H. Dalla-Torre, H. Van Swygenhoven, and M. Victoria, Acta Mater. **50**, 3957 (2002).
[47] M. A. Meyers, in *Dynamic Behavior of Materials* (John Wiley & Sons, Hoboken, 1994), p. 474.
[48] P. Landau, R. Z. Shneck, G. Makov, and A. Venkert, IOP Conf. Ser.: Mater. Sci. Eng. **3**, 012004 (2009).
[49] *Electron Backscatter Diffraction in Materials Science*, edited by A. J. Schwartz, M. Kumar, B. L. Adams, and D. P. Field (Springer US, Boston, MA, 2000), 1st ed., Vol. 339, pp. XVI; L. Vinet and A. Zhedanov, J. Phys. A **44**, 085201 (2011).
[50] A. Bhattacharyya, Bull. Calcutta Math. Soc. **35**, 99 (1943).